

## Signatures of valence fluctuations in CeCu<sub>2</sub>Si<sub>2</sub> under high pressure

Alexander T. Holmes\* and Didier Jaccard†

*Département de Physique de la Matière Condensée, Section de Physique, University of Geneva, 24 quai Ernest-Ansermet, CH-1211 Genève 4, Switzerland*

Kazumasa Miyake‡

*Division of Materials Physics, Department of Physical Science, Graduate School of Engineering Science, Osaka University, Toyonaka, Osaka 560-8531, Japan*

(Received 30 May 2003; published 15 January 2004)

Simultaneous resistivity and ac specific heat measurements have been performed under pressure on single-crystalline CeCu<sub>2</sub>Si<sub>2</sub> to over 6 GPa in a hydrostatic helium pressure medium. A series of anomalies was observed around the pressure coinciding with a maximum in the superconducting critical temperature,  $T_c^{\max}$ . These anomalies can be linked with an abrupt change of the Ce valence and suggest a second quantum critical point at a pressure  $P_v \approx 4.5$  GPa, where critical valence fluctuations provide the superconducting pairing mechanism, as opposed to spin fluctuations at ambient pressure. Such a valence instability—and associated superconductivity—is predicted by an extended Anderson lattice model with Coulomb repulsion between the conduction and  $f$  electrons. We explain the  $T$ -linear resistivity found at  $P_v$  in this picture, while other anomalies found around  $P_v$  can be qualitatively understood using the same model.

DOI: 10.1103/PhysRevB.69.024508

PACS number(s): 74.70.Tx

### I. INTRODUCTION

Boosted by the discovery of superconductivity in CeCu<sub>2</sub>Si<sub>2</sub> over 20 years ago,<sup>1</sup> the relationship between superconductivity and magnetism has been extensively investigated in various  $d$  and  $f$  heavy fermion (HF) compounds. A consensus has developed that HF superconductivity is mediated by spin fluctuations,<sup>2–5</sup> mainly because superconductivity was found close to a magnetic instability at  $T=0$ , sometimes described as a quantum critical point (QCP), often attained by applying pressure. A recent development is that an essentially gapless superconducting (SC) state has been identified by NMR and nuclear quadrupole resonance (NQR) measurements in the region where the SC state coexists with antiferromagnetism,<sup>6,7</sup> consistent with a theoretical prediction.<sup>8</sup>

In this paper we further explore the possibility that at a pressure  $P_v \approx 4.5$  GPa, a second QCP, associated with the  $f$  electron occupation number, has a major role to play in the superconductivity of CeCu<sub>2</sub>Si<sub>2</sub> and related compounds.<sup>9,10</sup>

CeCu<sub>2</sub>Si<sub>2</sub> has a superconducting ground state at ambient pressure with a critical temperature  $T_c$ , around 0.7 K. It is firmly believed that the compound is close to an antiferromagnetic QCP at slight negative pressure, accessible, for example, by partial substitution of Si with Ge.<sup>11</sup> When pressure is applied,  $T_c$  initially remains close to its ambient pressure value, followed by a sudden increase to around 2 K at about 3 GPa. A further increase in pressure results in a slower suppression of  $T_c$  to zero. This non monotonous behavior of  $T_c(P)$  was first explored by resistivity in the quasihydrostatic conditions of the Bridgman anvil cell.<sup>12</sup> Subsequent investigations by susceptibility<sup>13</sup> and resistivity<sup>14,15</sup> were carried out in various pressure media and showed considerable variation in  $T_c$  between samples, especially at high pressure.

With increasing pressure CeCu<sub>2</sub>Si<sub>2</sub> passes from a nearly trivalent  $4f^1$  behavior, with Kondo coupling between con-

duction and  $f$  electrons, to behavior at very high pressure characteristic of intermediate valence (IV) systems, whose valence fluctuates between the  $4f^n$  and  $4f^{n-1} + [5d6s]$  electronic configurations. As a result, deep in this IV regime, the resistivity, for instance, resembles that of LaCu<sub>2</sub>Si<sub>2</sub>, which lacks  $4f$  electrons. A similar  $T_c(P)$  dependence to that found in CeCu<sub>2</sub>Si<sub>2</sub> is seen in the isoelectronic sister compound CeCu<sub>2</sub>Ge<sub>2</sub>, offset by about 10 GPa due to the larger atomic volume of Ge.<sup>16</sup> Apart from this shift of the pressure scale, the two compounds share the same phase diagram.

From a more theoretical point of view, there exist at least three reasons to believe that critical valence fluctuations are at the origin of the pressure-induced peak of the SC transition temperature  $T_c$ .

First, the  $A$  coefficient of the  $T^2$  resistivity law decreases drastically by about two orders of magnitude around the pressure corresponding to the  $T_c$  peak.<sup>10</sup> Since  $A$  scales as  $(m^*/m)^2$  in the so-called Kondo regime, this implies that the effective mass  $m^*$  of the quasiparticles also decreases sharply there. This fall of  $m^*$  is possible only if there is a sharp change of Ce valence, deviating from Ce<sup>3+</sup>, since the following approximate formula for the renormalization factor  $q$  holds in the strongly correlated limit.<sup>17,18</sup>

$$\frac{m^*}{m} \approx q^{-1} = \frac{1 - n_f/2}{1 - n_f}, \quad (1)$$

where  $n_f$  is the  $f$  electron number per Ce ion.

Second, the so-called Kadowaki-Woods (KW) ratio<sup>19</sup>  $A/\gamma^2$ , where  $\gamma$  is the Sommerfeld coefficient of the electronic specific heat, crosses over quickly from that of a strongly correlated class to a weakly correlated one.<sup>20</sup> The inverse of the Sommerfeld coefficient,  $\gamma^{-1}$ , scales with the Kondo temperature  $T_K$ , which is experimentally accessible by resistivity measurements. This indicates that the mass en-

TABLE I. Anomalies in CeCu<sub>2</sub>Si<sub>2</sub> and CeCu<sub>2</sub>Ge<sub>2</sub> associated with valence transition, with references. Symbols explained in the text. Part (i): direct evidence for sudden valence change. Part (ii): Anomalies explained by published valence fluctuation theory (Refs. 21 and 22). Part (iii): anomalies explained by extended treatment of the critical valence fluctuations (Sec. IV). Part (iv): other anomalies observed around crossover to intermediate valence with pressure.

	CeCu <sub>2</sub> Si <sub>2</sub> Ref.	CeCu <sub>2</sub> Ge <sub>2</sub> Ref.
(i) Volume discontinuity	-	23
$L_{III}$ x-ray absorption	24	-
Drastic change of $A$ by two orders of magnitude	This work, 10	10
Change of $A \propto (T_1^{\max})^{-2}$ scaling	This work, 10	10
(ii) Maximum in $T_c(P)$	This work, 12	16
Large peak in $\rho_0$	This work, 10	10
(iii) Maximum in $\gamma \simeq (C_p/T)$	This work, 14	-
$\rho \propto T^n$ from $T_c < T < T^*$ , with $n(P_v) = 1$ minimum	This work, 12,25	10
(iv) Sample dependence of $T_c$	This work, 10,12,13,15,26,27	10
Enhanced $\frac{\Delta C_p}{\gamma T} \Big _{T_c}$	This work	-
Resistivity and thermopower indicate $T_1^{\max} \simeq T_2^{\max}$	10,25	10,28
Broad superconducting transition widths $\Delta T_c$	This work, 12	10

hancement due to the dynamical electron correlation is quickly lost at around  $P \sim P_v$ , in agreement with the previous point. The phenomenon can be understood if we note the fact that  $\gamma$  consists essentially of two terms:

$$\gamma = \gamma_{\text{band}} \left( 1 - \frac{\partial \Sigma(\epsilon)}{\partial \epsilon} \right) \equiv \gamma_{\text{band}} + \gamma_{\text{cor}}, \quad (2)$$

where  $\gamma_{\text{band}}$  is due to the so-called band effect and  $\gamma_{\text{cor}} \equiv -\gamma_{\text{band}} \partial \Sigma(\epsilon) / \partial \epsilon$  is due to the many-body correlation effect, with  $\Sigma(\epsilon)$  being the self-energy of the correlated electrons.  $\gamma_{\text{cor}}$  and  $A$  are related to each other through the Kramers-Kronig relation, leading to a large value of the KW ratio,<sup>20</sup> and when  $\gamma_{\text{cor}} \gg \gamma_{\text{band}}$ , this is indeed seen. On the other hand, if  $\gamma_{\text{cor}} \sim \gamma_{\text{band}}$ , the ratio  $A/\gamma^2$  should be reduced from the KW value considerably because the effect of  $\gamma_{\text{band}}$  cannot be neglected in its denominator.

Third, there is a sharp peak in the residual resistivity  $\rho_0$  at around  $P \simeq P_v$ ,<sup>10</sup> which can be understood as a many-body effect enhancing the impurity potential (in fact we define the pressure  $P_v$  experimentally by the maximum of  $\rho_0$ ). In the forward scattering limit, this enhancement is proportional to the valence susceptibility  $-(\partial n_f / \partial \epsilon_f)_\mu$ , where  $\epsilon_f$  is the atomic  $f$  level of the Ce ion and  $\mu$  is the chemical potential.<sup>21</sup> Physically speaking, local valence change coupled to the impurity or disorder gives rise to a change of valence in a wide region around the impurity which then scatters the quasiparticles quite strongly, leading to an increase of  $\rho_0$ . The enhancement of  $\rho_0$  can be thus directly related to the degree of sharpness of the valence change, because the variation of the atomic level  $\epsilon_f$  is considered to be a smooth function of the pressure.

These circumstantial clues to the importance of critical valence fluctuations have been backed up by a microscopic calculation of  $T_c$  for  $d$ -wave pairing as a function of  $\epsilon_f$ .<sup>22</sup> This showed that sudden valence change occurs if a moderately sized Coulomb repulsion  $U_{cf}$  is taken into account between the conduction  $c$ - and localized  $f$  electrons, with the peak structure of  $T_c$  being qualitatively reproduced.

Table I summarizes the current experimental evidence of anomalies seen in CeCu<sub>2</sub>(Ge/Si)<sub>2</sub> around  $P_v$ .

Part (i) of Table I refers to direct evidence for a valence transition of the Ce ion: Cell volume<sup>23</sup> and  $L_{III}$  x-ray absorption<sup>24</sup> measurements show discontinuities as a function of pressure. The drastic decrease of the  $A$  coefficient of the  $T^2$  resistivity law, along with the  $A$  vs  $T_1^{\max}$  scaling relation, indicates that the system is leaving the strongly correlated regime characterized by an  $f$  occupation number close to unity. ( $T_1^{\max}$  is defined in Fig. 5 and assumed to be proportional to  $T_K$ .)

Part (ii) refers to anomalies observed close to the maximum of  $T_c$  predicted by critical valence fluctuation theory.<sup>21,22</sup> These are the maximum of  $T_c$  itself and the enhanced residual resistivity  $\rho_0$ .<sup>10,12-16</sup>

Part (iii) refers to properties following from the extended treatment of the critical valence fluctuations found in Sec. IV of this paper. This includes the linear resistivity<sup>10</sup> and the maximum in  $\gamma$ , both found around  $P_v$ .

In part (iv) are listed the remaining features that are observed in CeCu<sub>2</sub>Si<sub>2</sub> and CeCu<sub>2</sub>Ge<sub>2</sub> around the maximum in  $T_c$  but which are so far not fully explained—for example the merging of  $T_1^{\max}$  and  $T_2^{\max}$ , where the latter (also defined in Fig. 5) is believed to reflect the effect of the excited crystal-line electric field (CEF) split  $f$  levels. Many of the anomalies noted in table I have also been observed to coincide with the maximum of  $T_c$  in other HF superconductors, from CePd<sub>2</sub>Si<sub>2</sub>

(Ref. 29) to CeCu<sub>5</sub>Au (Ref. 30), the latter showing traces of superconductivity under pressure.

Previous work on CeCu<sub>2</sub>Si<sub>2</sub> has shown a lot of variation in low-temperature behavior between different samples. The fact that not all reports have shown every anomaly is not entirely surprising, since large variations in the electronic properties of CeCu<sub>2</sub>Si<sub>2</sub> are well known to result from extremely small differences in composition.<sup>31–33</sup> The extension of these variations with pressure has not been systematically explored, but almost all samples so far studied have shown an enhancement of  $T_c$ , along with effects such as the enhancement of the residual resistivity, to be discussed below.

This variability under pressure may be due to the samples themselves or to pressure inhomogeneities caused by nonhydrostatic pressure media. We were therefore motivated to use solid helium as a pressure medium, due to its near-ideal hydrostaticity at low temperature. By simultaneously probing resistivity and specific heat in the same sample, we were able to explore both percolative transport and bulk evidence for superconductivity.

## II. EXPERIMENTAL METHODS

High pressure was induced using diamond anvils with a 1.5-mm culet.<sup>34</sup> A stainless steel gasket was specially prepared to absorb the large volume decrease of the helium pressure medium from ambient pressure and to avoid severing the measurement wires. These were insulated from the gasket using a mixture of Al<sub>2</sub>O<sub>3</sub> powder and epoxy resin. The pressure was measured to within 0.02 GPa at various temperatures down to 4.2 K using the ruby fluorescence scale.

The CeCu<sub>2</sub>Si<sub>2</sub> sample was prepared by reaction of its constituent elements with a slight excess of Cu, with a nominal initial composition CeCu<sub>2.1</sub>Si<sub>2</sub>. The product was then melted in an induction furnace and slowly allowed to crystallize under 50 bars Ar in a BaZrO<sub>3</sub> crucible (see Ref. 14 for more details).

The small monocrystal used in this work was cut and polished to 230×80×20 μm<sup>3</sup>, and six 5 μm  $\phi$  wires (four gold and two Au+0.07 at.% Fe) were spot welded to the sample. The  $c$  axis of the tetragonal structure was parallel to its smallest dimension. The magnetic field, when applied, was parallel to the  $c$  axis.

The six wires spot-welded to the sample allowed multiple redundant measurements to be performed. This improved reliability and enabled us to verify the calorimetry measurements using several different configurations. The sample resistance could be measured by a four-point method; knowledge of the sample dimensions then enabled the absolute resistivity to be determined to within 10%.

The two thermocouple junctions were formed from an Au/AuFe pair at either end of the sample. An alternating resistive heating current was passed through one (to avoid passing the current through the sample), while the signal from the other was measured using a lock-in amplifier. The resulting temperature oscillations serve as a sensitive measure of the sample heat capacity.<sup>35</sup> A simple model of the ac

calorimetry system predicts the amplitude and phase of the temperature oscillations ( $T_{ac}$ ) induced by ac heating:

$$T_{ac} = \frac{P_0}{K + i\omega C}, \quad (3)$$

where  $P_0$  is the heating power,  $K$  the thermal conductance to the bath,  $C$  the heat capacity, and  $\omega/2\pi$  the excitation frequency, assumed to be low enough that the thermometer can follow the temperature oscillations (the factor of  $2\pi$  may be assumed implicitly from this point). The signal therefore contains a contribution from the specific heat and from thermal coupling to the surroundings.

For frequencies  $\omega \gg \omega_c$ , where  $\omega_c$  is the cutoff frequency  $K/C$ , the sample contribution dominates the signal, and  $|T_{ac}|$  can be considered to be inversely proportional to the heat capacity (which we assume to be dominated by the sample). For  $\omega \ll \omega_c$ , the signal approaches the dc limit and gives a measure of the mean elevation of the sample temperature over that of the bath. For intermediate measuring frequencies, information from the phase  $\theta$  can be used to extract the specific heat:

$$C = \frac{-P_0 \sin \theta}{\omega |T_{ac}|}. \quad (4)$$

Alternatively, one can subtract a background signal taken at a different frequency, with

$$C = \frac{P_0}{(\omega_2^2 - \omega_1^2)^{1/2}} \left( \frac{1}{|T_{ac, \omega_2}|^2} - \frac{1}{|T_{ac, \omega_1}|^2} \right)^{1/2}, \quad (5)$$

where ideally  $\omega_2 > \omega_c > \omega_1$ . The sample temperature must also be corrected for the constant dc component of the oscillatory Joule heating. This was done by repeating the measurement well below the cutoff frequency, also providing the background signal in order to estimate  $C_p$  using Eq. (5). Raw and processed ac calorimetry data can be compared at one pressure in Ref. 36.

The cutoff frequency  $\omega_c$  turned out to be very temperature dependent, varying between 200 Hz at 0.5 K and over 2 kHz at 1.5 K, presumably due to the thermal properties of the surrounding material. Fortunately, while complicating the data analysis, the reduction in  $\omega_c$  at the lowest temperatures allows the technique to be used down to  $\sim 100$  mK. The two estimates of  $C_p$  using Eqs. (4) and (5) are in good agreement below  $\sim 2$  K. The working frequency  $\omega_2$  was generally of the order of  $\omega_c$ .

Sources of systematic error in the result might come from: variation of the AuFe thermopower under pressure; temperature- and/or frequency-dependent addenda to the measured specific heat due to the pressure medium, gasket, and/or anvils; or any irreversibility or first-order character in the transitions being observed. These potential problems will be addressed in the discussion.

## III. EXPERIMENTAL RESULTS

We present five principal results from the sample reported in this paper, and by drawing on previous work, we aim to

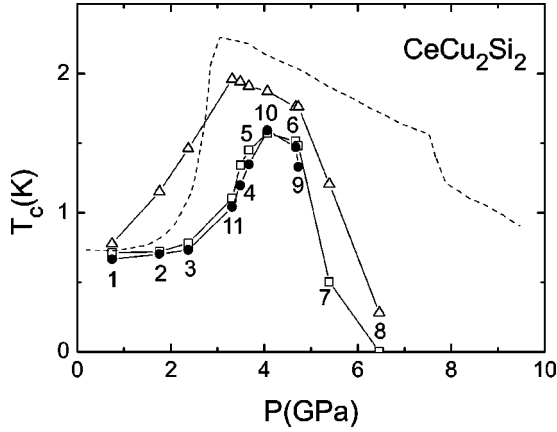


FIG. 1.  $T_c(P)$  in  $\text{CeCu}_2\text{Si}_2$  determined from resistivity and specific heat measurements. The triangles show  $T_c$  determined from the onset of the resistive transition ( $T_c^{\text{onset}}$ ), the squares show its completion ( $T_c^{R=0}$ ), and the solid circles show the midpoint of the specific heat jump. The numbers indicate the sequence of pressures. The dotted line shows  $T_c$  determined by susceptibility in a different sample, also in a helium pressure medium (Ref. 13).

place our work in a broader context. We will try to highlight common features found in many samples of  $\text{CeCu}_2\text{Si}_2$ , one of the defining characteristics of which is its variability.

(i) We present the superconducting phase diagram obtained using various criteria for  $T_c$  and compare it to the widely quoted phase diagram determined under hydrostatic conditions by susceptibility.

(ii) We examine the details of the superconducting transition, which provides some insight into the nature of the SC state and into the sample itself.

(iii) We estimate the variation of the Sommerfeld coefficient  $\gamma$ , with pressure, and compare it to previous results obtained by analysis of the upper critical field.

(iv) We report the pressure dependence of the residual resistivity  $\rho_0$  and exponent  $n$  determined by a fit to the normal-state resistivity of  $\rho = \rho_0 + \tilde{A}T^n$  ( $\tilde{A}$  denoting a free exponent as opposed to the quadratic coefficient  $A$ ). A comparison of  $\rho_0(P)$  between different samples reveals a scaling relation which can be related to the theoretical enhancement of impurity scattering.

(iv) We explore the deviation from the scaling relation  $A \propto T_K^{-2}$ , which indicates a sharp change in the  $f$  electron occupation number described in the Introduction. The enhancement of  $T_c$  and the other results described above is shown to occur around the same pressure.

Figure 1 shows the superconducting phase diagram determined by both resistivity and specific heat, both on increasing and decreasing the pressure. Two qualitatively different types of behavior can be seen in the same sample, represented by the onset and completion of the resistive transition.

If we follow the transition onset  $T_c^{\text{onset}}(P)$ , one sees sharp kinks similar to those seen in Ref. 13 (dashed line), along with a linear decrease of  $T_c$  between 3.3 and 4.8 GPa at a rate of  $0.14 \text{ K GPa}^{-1}$ . Superconductivity is observed, however, over a much smaller pressure range in our sample than in Ref. 13.

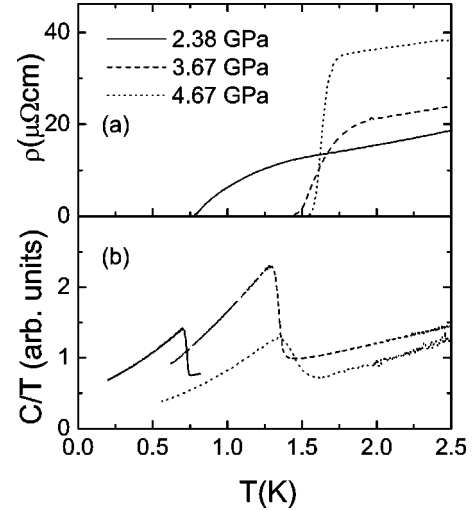


FIG. 2. Superconducting transition at three pressures in (a) resistivity and (b) specific heat. Note the width of the resistive transitions and the fact that the start of the jump in specific heat coincides with the completion of the resistive transition.

The temperature  $T_c^{R=0}(P)$ , at which the resistance vanishes, behaves differently from  $T_c^{\text{onset}}(P)$ . It has a narrower peak with a maximum at slightly higher pressure.  $T_c^{R=0}$  agrees closely, however, with the transition seen in the specific heat (see below). When a magnetic field was applied,  $T_c^{R=0}$  and the specific heat anomaly shifted in agreement.

The large resistive transition widths found in  $\text{CeCu}_2\text{Si}_2$  at high pressure are often blamed on a lack of hydrostaticity due to the pressure medium. As helium was used in this case, we can rule out pressure inhomogeneities and concentrate on the sample itself. Further information about the SC state comes from the effect of measurement current on the transition width. For example, at 1.78 GPa high current led to the upper part of the transition disappearing, and a resistive transition can even be recovered with a narrow width comparable to that close to ambient pressure. This is presumably due to the presence of filamentary superconductivity, with a higher  $T_c$ , whose critical current density is exceeded. These broad resistive transitions appear to be a universal feature of  $\text{CeCu}_2\text{Si}_2$  at high pressure. Let us recall that even for the highest  $T_c^{\text{onset}}$  measured in a single crystal, at 2.4 K, a tail of 1% of the normal-state resistivity remained well below 2 K, vanishing only at 1.5 K.<sup>14</sup> The status of the superconductivity of  $\text{CeCu}_2\text{Si}_2$  between  $T_c^{\text{onset}}$  and  $T_c^{R=0}$  remains mysterious.

Figure 2 compares the superconducting transition in resistivity and specific heat at three different pressures. At 2.38 GPa the resistive transition is broad and the sharp specific heat jump at 0.73 K begins at the point where the resistance falls to zero. At 3.67 GPa the specific heat jump, at 1.35 K, is much larger and remains sharp (and did so at intervening pressures), while the corresponding resistive transition has narrowed considerably. At 4.07 GPa (not shown) where  $T_c^{R=0}$  has a maximum around 1.6 K in both  $\rho$  and  $C_P$ , the specific heat peak has already started to broaden and collapse in amplitude, while at the same pressure the resistive transi-

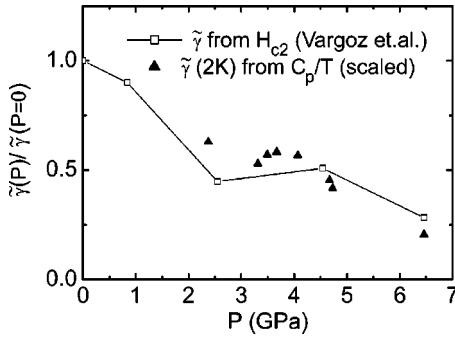


FIG. 3. Estimate  $\tilde{\gamma}(P)$  of the Sommerfeld coefficient from an ac calorimetry signal at 2 K (triangles), scaled for comparison with that deduced from  $H_{c2}$  measurements (squares) (Ref. 14). The noise on the calorimetry signal is smaller than the symbol size; however, see text for a discussion of possible systematic errors.

tion is at its narrowest since ambient pressure. As  $T_c$  is driven to zero at high pressure, the superconducting  $C_p$  jump becomes smaller and broader (as shown at 4.67 GPa) until it is no longer visible. When the pressure was reduced, the  $C_p$  peak recovered its shape, indicating the reversibility of the bulk pressure-induced behavior.

The dramatic increase in the apparent size of the superconducting jump is intriguing and might suggest the presence of strong coupling<sup>37</sup> or other qualitative change in the SC state. Although the apparent value of  $(\Delta C_p/\gamma T)_{T_c}$  is clearly less than the BCS ratio of 1.43, similar ac measurements on CeCoIn<sub>5</sub> in an argon pressure medium indicate that there is a substantial contribution to the measured heat capacity from addenda.<sup>38</sup> In helium we would expect this to be even more significant

The increase in the  $C_p$  jump size might itself be an artifact of the uncalibrated ac calorimetry method; nevertheless,  $(\Delta C_p/\gamma T)_{T_c}$  does appear to show a maximum at a pressure coinciding with the increase in  $T_c$ . Furthermore, the assumption of strong coupling provided the best fit to  $H_{c2}$  for measurements of the upper critical field in another sample.<sup>14</sup>

The electronic specific heat coefficient  $\gamma$  and, hence, the effective mass  $m^*/m$  can be estimated by following the calorimetric signal  $C/T$  at a fixed temperature and measurement frequency above the superconducting transition, though this includes constant or slowly varying addenda from the helium, diamonds, etc. Figure 3 shows the estimate  $\tilde{\gamma}(P)$ , along with the value deduced from measurements of the upper critical field in Ref. 14. A single constant scale factor has been introduced, showing that the two curves can be superimposed. There is a clear anomaly in  $\tilde{\gamma}$  at 4 GPa (just below the pressure corresponding to  $T_c^{\max}$ ), superimposed on a constant reduction with pressure. The effective mass is also reflected in the initial slope of the upper critical field  $H_{c2}'(T_c)$ , which in our sample also had a maximum at the same pressure as the peak in  $\tilde{\gamma}$ .

The residual resistivity  $\rho_0$  has a huge peak at a pressure slightly higher than the maximum in  $T_c$ . The magnitude of this peak varies by a factor of more than 10 between samples.<sup>27,14</sup> However, it is possible to scale the residual re-

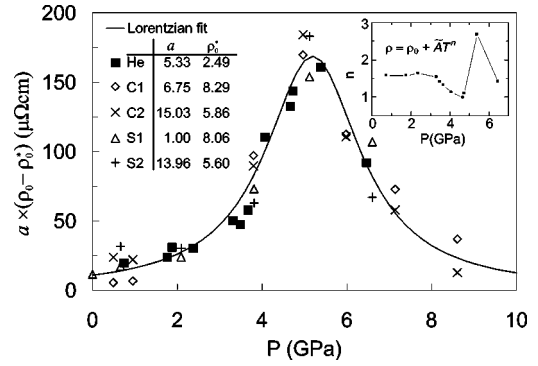


FIG. 4. Enhancement of residual resistivity in several different CeCu<sub>2</sub>Si<sub>2</sub> samples, scaled to a universal pressure dependence, with  $a$  and  $\rho_0^*$  being normalizing factors. The maximum in  $\rho_0$  is at a pressure slightly higher than that corresponding to the maximum in  $T_c$ . The inset shows  $n$  for a fit of  $\rho = \rho_0 + \tilde{A}T^n$ . Solid squares indicate results from this work; the rest are reported in Ref. 27 (S and C refer to the original labels and a retained for continuity).

sistivities from different samples onto the same Lorentzian curve (see Fig. 4). A constant value  $\rho_0^*$ , different for each sample, is subtracted from  $\rho_0$  at each pressure, and the result is multiplied by a scale factor  $a$  [i.e.,  $\rho_0' = a(\rho_0 - \rho_0^*)$ ], so that all lie on the curve defined by sample S1, which has the highest residual resistivity (i.e.,  $a_{S1} = 1$ ).

According to the theoretical prediction, the residual resistivity  $\rho_0$  is given as<sup>21</sup>

$$\rho_0 = B n_{\text{imp}} |u(0)|^2 \ln \left| \left( -\frac{\partial n_f}{\partial \epsilon_f} \right)_\mu \right| / N_F + \rho_0^{\text{unit}}, \quad (6)$$

where the coefficient  $B$  depends on the band structure of host metals,  $n_{\text{imp}}$  is the concentration of impurities with moderate scattering potential  $u(q)$  coming from disorder other than Ce ions,  $N_F$  is the density of states of quasiparticles around the Fermi level, and the last term represents the residual resistivity due to unitary scattering mainly arising from any deficit or defect of the Ce ions. The scaling behavior of  $\rho_0$  shown in Fig. 4 would be possible if the universal form is given by  $\ln |(-\partial n_f/\partial \epsilon_f)_\mu/N_F|$ . It is an open question whether the observed Lorentzian form is indeed reproduced by the theory of Ref. 22.

There is a striking correlation between the scaling factor  $a$  and the behavior of  $T_c$ . The sample measured in helium reported in this paper and sample C1, pressurized in steatite, both have similar values of  $a$ , and both  $T_c^{\text{onset}}$  and  $T_c^{R=0}$  agree over almost the entire pressure range. Sample S1, with the highest  $\rho_0$  at  $P_0$ , has a lower  $T_c^{\max}$  ( $\approx 1.2$  K), and the superconductivity disappears at a lower pressure. Samples C2 and S2 have scaling factors  $a$  around 14, and show a higher maximum  $T_c$ , with superconductivity extended over a greater pressure range than in the samples with larger residual resistivities. These differences between samples, both in  $\rho_0$  and  $T_c$ , are vastly amplified from their appearance at ambient pressure. According to Eq. (6), the scaling factor  $a$  is

proportional to the concentration of impurities. Our observations suggest therefore that these have a significant pair-breaking effect.

The inset in Fig. 4 shows the result of a fit to  $\rho = \rho_0 + \tilde{A}T^n$  between  $T_c$  and 4.2 K. There are two important points to note here. First, at a pressure slightly higher than the maximum  $T_c$ ,  $\rho(T)$  is linear in  $T$  up to about 25 K. Second, the exponent appears surprisingly large ( $n \approx 2.7$ ) at a slightly higher pressure corresponding to the maximum  $\rho_0$ . This is difficult to understand without taking into account the resistivity due to impurity scattering. In sample S1, reported in Ref. 26, the residual resistivity reaches  $\sim 160 \mu\Omega \text{ cm}$  at  $P_v$ , compared to a maximum of  $35 \mu\Omega \text{ cm}$  for the sample reported here.  $\rho(T)$  then showed a falloff with temperature very similar to that of a Kondo impurity system. In other samples, this behavior is hidden by the usual positive temperature dependence of the resistivity. Contrary to the usual situation, where the lowest  $\rho_0$  possible is sought, this example shows how samples whose residual resistivities are large at ambient pressure can reveal interesting physics at high pressure. Even if a negative temperature dependence is not seen, the power-law fit to the resistivity is affected, deviating from the linear relationship predicted in Sec. IV and leading to anomalous values of  $n$ . At lower pressure, the  $\tilde{A}$  coefficient is an order of magnitude larger, so (for example) almost linear resistivity is observed at a pressure corresponding to  $T_c^{\text{max}}$ . Note that a quadratic temperature dependence of  $\rho$  was recovered at the lowest temperatures when superconductivity was suppressed by a magnetic field greater than  $H_{c2}$ .

The normal-state resistivity of heavy fermions can usually be understood in terms of the Kondo lattice model.<sup>39</sup> At high temperature the  $f$ -electron moments are localized and disordered, and the resistivity is large and dominated by the scattering from spin disorder, with a characteristic  $-\ln T$  slope. As the temperature is reduced, Kondo singlets form below a characteristic temperature  $T_K$ , and coherence effects in the periodic lattice cause the resistivity to drop below a maximum, at  $T_1^{\text{max}}$ , which can be considered as proportional to  $T_K$ . For  $T \ll T_K$  away from the critical point, Fermi-liquid-like behavior is recovered, with  $\rho \sim AT^2$ , where  $A \propto T_K^{-2}$  and reflects the hugely enhanced effective mass caused by interactions between the  $f$  electrons. In a real system where  $T_K$  is not too large, a second peak in the resistivity occurs at  $T_2^{\text{max}} > T_1^{\text{max}}$ , due to the CEF effect<sup>40,41</sup> (see inset of Fig. 5). The low-temperature behavior then reflects the characteristics of the lowest CEF-split  $f$  level. When pressure is applied,  $T_2^{\text{max}}$  remains fairly constant, while  $T_K$  rapidly increases, seen via the rise in  $T_1^{\text{max}}$ . When  $T_K > \Delta_{\text{CEF}}$  ( $\Delta_{\text{CEF}}$  is the CEF splitting between the ground and excited states) the full six-fold degeneracy of the  $J=5/2$   $4f^1$  multiplet is recovered, even at the lowest temperatures. As a result the resistivity maxima at  $T_1^{\text{max}}$  and  $T_2^{\text{max}}$  merge into a single peak.<sup>10</sup> Similar behavior in the magnetic component of the resistivity is found in all Ce compounds studied [such as CeCu<sub>5</sub>Au (Ref. 30), CePd<sub>2</sub>Si<sub>2</sub> (Ref. 29), CePd<sub>2</sub>Ge<sub>2</sub> (Ref. 42)].

In Fig. 5 the  $A$  vs  $T_1^{\text{max}}$  scaling is explored in both CeCu<sub>2</sub>Si<sub>2</sub> and CeCu<sub>2</sub>Ge<sub>2</sub>. The value of  $A$  was determined

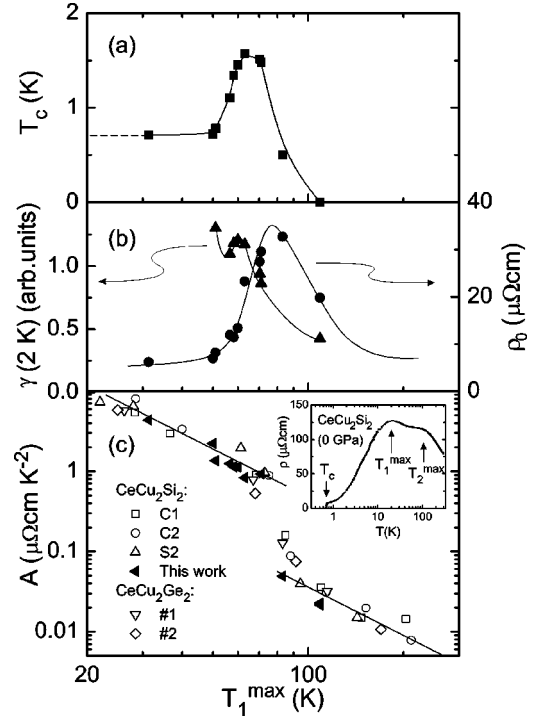


FIG. 5. Plotted against  $T_1^{\text{max}}$  (defined in inset), a measure of the characteristic energy scale of the system, are (a) the bulk superconducting transition temperature, (b) the residual resistivity and estimate  $\tilde{\gamma}$  of the Sommerfeld coefficient, and (c) the coefficient  $A$  of the  $\rho \sim AT^2$  law of resistivity, including data from CeCu<sub>2</sub>Ge<sub>2</sub>. Note the straight lines where the expected  $A \propto (T_1^{\text{max}})^{-2}$  scaling is followed. The maximum of  $T_c$  coincides with the start of the region where the scaling relation is broken, while the maximum in residual resistivity is situated in the middle of the collapse in  $A$ . Pressure increases towards the right-hand side of the scale (high  $T_1^{\text{max}}$ ).

from the slope of the normal-state resistivity versus  $T^2$ , despite the non-Fermi-liquid behavior shown in the inset of Fig. 4. However, if one allows the exponent  $n$  to vary between 1 and 2, the resulting coefficient will not vary more than a factor of 2, which is within the scatter of the data. There are two regions where the predicted  $A \propto (T_1^{\text{max}})^{-2}$  relationship is followed, separated by an abrupt drop in  $A$  of over an order of magnitude. The collapse of  $A$  seems closely connected with the enhancement of superconductivity, it is at the start of this drop that  $T_c$  has a maximum, and the superconductivity has disappeared by the point where the  $A \propto (T_1^{\text{max}})^{-2}$  scaling is recovered. The residual resistivity however, peaks at around the midpoint of the drop in  $A$ , and this is the point where  $P_v$  is defined.

#### IV. THEORY OF $T$ -LINEAR RESISTIVITY AND ENHANCED SOMMERFELD COEFFICIENT

Various unconventional properties observed around  $P \sim P_v$  have been explained, at least qualitatively, by a series of theoretical investigations based on an extended Anderson lattice model.<sup>21,22,43</sup> However, the  $T$ -linear temperature dependence of the resistivity observed in a narrow region around  $P \sim P_v$  remains as yet unexplained. In Ref. 22, mi-

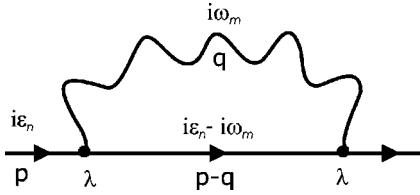


FIG. 6. Feynman diagram for the self-energy given by Eqs. (9) and (10). The solid line represents the Green function of the quasiparticles, the wavy line the propagator of the valence fluctuations, and the solid circle the coupling between valence-fluctuation modes and the quasiparticles.  $\varepsilon_n$  and  $\omega_m$  are the Matsubara frequency of the quasiparticle and fluctuation propagators, respectively.

microscopic calculations showed that the static limit of the effective interaction  $\Gamma^{(0)}(q)$  between quasiparticles is enhanced greatly around  $P \sim P_v$ , and is almost independent of  $q$ , the momentum transfer, up to  $\sim 3/2$  of  $p_F$ , reflecting the local nature of critical valence fluctuations. This implies that the valence fluctuation response function  $\chi_v(q, \omega)$ , is also almost  $q$  independent in the low-frequency region. Based on this observation, we present here a phenomenological theory explaining the  $T$ -linear resistivity and the enhancement of the Sommerfeld coefficient  $\gamma$  around  $P \sim P_v$ .

We adopt an exponentially decaying phenomenological form for the valence-fluctuation propagator (dynamical valence susceptibility)  $\chi_v$ :

$$\chi_v(q, \omega) \equiv i \int_0^\infty dt e^{i\omega t} \langle [n_f(q, t), n_f(-q, 0)] \rangle \quad (7)$$

$$= \frac{K}{\omega_v - i\omega}, \quad \text{for } q < q_c \sim p_F, \quad (8)$$

where  $n_f(q)$  is the Fourier component of the number of  $f$  electrons per Ce site,  $K$  is a constant of  $\mathcal{O}(1)$ , and  $\omega_v$  parametrizes the closeness to criticality.  $\omega_v$  is inversely proportional to the valence susceptibility  $\chi_v(0, 0) = -(\partial n_f / \partial \varepsilon_f)_\mu$ .

The real and imaginary parts of the retarded self-energy  $\Sigma_{vf}^R(p, \varepsilon + i\delta)$ , respectively, give a measure of the quasiparticle effective mass and lifetime. They can be calculated using a simple one-fluctuation mode exchange process (see Fig. 6) and are given as follows:

$$\begin{aligned} \text{Re}\Sigma_{vf}^R(p, \varepsilon) &= -\frac{K}{2\pi} \sum_{\mathbf{q}} |\lambda|^2 \int_{-\infty}^{+\infty} dx \frac{x}{\omega_v^2 + x^2} \\ &\quad \times \frac{\coth \frac{x}{2T} + \tanh \frac{\xi_{\mathbf{p}-\mathbf{q}}}{2T}}{-\varepsilon + \xi_{\mathbf{p}-\mathbf{q}} + x}, \end{aligned} \quad (9)$$

$$\begin{aligned} \text{Im}\Sigma_{vf}^R(p, \varepsilon) &= -\frac{K}{2} \sum_{\mathbf{q}} |\lambda|^2 \frac{\varepsilon - \xi_{\mathbf{p}-\mathbf{q}}}{\omega_v^2 + (\varepsilon - \xi_{\mathbf{p}-\mathbf{q}})^2} \\ &\quad \times \left( \coth \frac{\varepsilon - \xi_{\mathbf{p}-\mathbf{q}}}{2T} + \tanh \frac{\xi_{\mathbf{p}-\mathbf{q}}}{2T} \right), \end{aligned} \quad (10)$$

where  $\lambda$  is the coupling between quasiparticles and the valence fluctuation modes, and  $\xi_p$  is the dispersion of the quasiparticle. For simplicity,  $\lambda$  is assumed to be constant without wave number or frequency dependence.

In typical limiting cases, Eq. (10) can be straightforwardly calculated in the approximation  $\xi_{\mathbf{p}-\mathbf{q}} \approx -vq \cos \theta$ , where  $\theta$  is the angle between  $\mathbf{p}$  and  $\mathbf{q}$ ,  $v$  is the quasiparticle velocity, and  $p$  is assumed to be on the Fermi surface, i.e.,  $p = p_F$ :  $T = 0$ ,  $\varepsilon \neq 0$ :

$$\text{Im}\Sigma_{vf}^R(p_F, \varepsilon) \approx -\frac{|\lambda|^2 K q_c^2}{32\pi^2 v} \ln \left( 1 + \frac{\varepsilon^2}{\omega_v^2} \right), \quad (11)$$

where  $q_c$  is the cutoff wave number of the order of  $k_F$ .  $\varepsilon = 0$ ,  $0 < T \ll \varepsilon_F$ :

$$\begin{aligned} \text{Im}\Sigma_{vf}^R(p_F, 0) &\approx -\frac{|\lambda|^2 K}{8\pi^2 v} \int_0^{q_c} dq q \int_{-vq/2T}^{vq/2T} dy \frac{y}{(\omega_v/T)^2 + y^2} \\ &\quad \times \left( \coth \frac{y}{2} - \tanh \frac{y}{2} \right), \end{aligned} \quad (12)$$

where  $y = vq \cos \theta / 2T$ . Since  $vq \gg T$  holds in the dominant region of  $q$  space, the integration with respect to  $y$  can be performed, to a good accuracy, leading to

$$\text{Im}\Sigma_{vf}^R(p_F, 0) \approx -\frac{|\lambda|^2 K q_c^2}{4\pi^2 v} \frac{T}{\omega_v} \tan^{-1} \frac{T}{\omega_v}, \quad (13)$$

where we have made approximation that the range of integration is restricted as  $-1 < y < 1$  in which the last factor in Eq. (12) is approximated as  $2/y$ . Then,

$$\text{Im}\Sigma_{vf}^R(p_F, 0) \approx -\frac{|\lambda|^2 K q_c^2}{4\pi^2 v} \begin{cases} \left( \frac{T}{\omega_v} \right)^2, & T \ll \omega_v \\ \frac{\pi}{2} \frac{T}{\omega_v}, & T \gg \omega_v \end{cases}. \quad (14)$$

The latter result  $\text{Im}\Sigma_{vf}^R(p_F, \varepsilon = 0) \propto T/\omega_v$ , for  $T \gg \omega_v$ , implies that almost all the critical valence-fluctuation modes can be regarded as classical at  $T > \omega_v$ , and  $T$ -linear dependence stems from the asymptotic form of  $\coth(x/2T) \approx 2T/x$ , essentially the classical approximation of the Bose distribution function.

The real part of the self-energy, Eq. (9), can be calculated easily at  $T = 0$  and  $\varepsilon \sim 0$ , leading to

$$\begin{aligned} \text{Re}\Sigma_{vf}^R(p_F, \varepsilon) - \Sigma_{vf}^R(p_F, 0) &= -\frac{|\lambda|^2 K \varepsilon}{4\pi^2} \int_0^{q_c} dq q^2 \int_{-1}^1 dt \left[ \frac{-1}{\omega_v^2 + (vqt)^2} \ln \left| \frac{e\omega_v}{vqt} \right| \right. \\ &\quad \left. + \frac{\pi \omega_v v q |t|}{[\omega_v^2 + (vqt)^2]^2} + \frac{2\omega_v^2}{[\omega_v^2 + (vqt)^2]^2} \ln \left| \frac{\omega_v}{vqt} \right| \right], \end{aligned} \quad (15)$$

where  $t = \cos \theta$ . In the limit  $\omega_v \ll v p_F$ , integration with respect to  $t$  in Eq. (15) leads to

$$\text{Re}\Sigma_{vf}^R(p_F, \epsilon) \simeq -\frac{|\lambda|^2 K q_c^2}{2\pi^2 v} \frac{\epsilon}{\omega_v} \int_0^1 du \frac{1-u^2}{u^2+1} \ln \left| \frac{1}{u} \right| \quad (16)$$

$$\propto -\frac{\epsilon}{\omega_v}, \quad (17)$$

where  $u = vqt/\omega_v$ .

The  $T$ -linear dependence of  $\text{Im}\Sigma_{vf}^R(p, 0)$ , for  $T > \omega_v$ , Eq. (14), implies  $T$ -linear resistivity, as the quasiparticles are subject to large-angle scattering by the critical valence-fluctuation modes. These are effective in a wide region in the Brillouin zone due to their local nature and easily couple to the umklapp process of quasiparticle scattering. This result is consistent with the experimental fact that  $T$ -linear resistivity is observed in a narrow pressure region around  $P_v$ , which is considered to correspond to a nearly critical valence transition of the Ce ion.

Such a  $T$ -linear dependence has been discussed in the context of high- $T_c$  cuprates with a marginal Fermi liquid (MFL) assumption,<sup>44</sup> and charge transfer fluctuations were once considered as an origin for MFL,<sup>45,46</sup> while further theoretical models have been put forth up to now.<sup>47</sup> Excepting the  $T$ -linear resistivity, the present result is different from MFL behavior. The self-energy exhibits different energy dependence, while the idea for the origin of our singular behavior shares aspects similar to the first idea of a charge transfer mechanism for high- $T_c$  cuprates.<sup>45,46</sup>  $\Sigma(\epsilon)$  in the MFL model is given as  $\Sigma(\epsilon) \propto (\epsilon \ln \epsilon - i|\epsilon|)$ ,<sup>44</sup> which is indeed different from the present case [Eqs. (11) and (17)]. In any case, it is to be noted that  $T$ -linear resistivity is accompanied by the peak of  $T_c$  in both systems, high- $T_c$  cuprates and  $\text{CeCu}_2\text{Si}_2$ .

The result (17) implies that the mass enhancement  $[1 - \partial \text{Re}\Sigma_{vf}^R(\epsilon)/\partial \epsilon]$  is expected around  $P \sim P_v$ . Namely, the effective mass is given by

$$m^* \propto \bar{m} \frac{1}{\omega_v}, \quad (18)$$

where  $\bar{m}$  is the effective mass renormalized by the conventional correlation effect, leading to heavy electrons—i.e., not including the effect of critical valence fluctuations. This latter effective mass  $\bar{m}$  exhibits a drastic decrease around  $P \sim P_v$ , while the second factor in Eq. (18) is enhanced. Both effects should be reflected in the Sommerfeld coefficient  $\gamma$ , so that the peak of  $\gamma \propto m^*$  is shifted to the lower-pressure (larger  $\bar{m}$ ) side, and the anomaly of  $\gamma$  due to the valence fluctuations may be smeared to some extent. Nevertheless, some trace should be observed. (The shift of peak of  $\gamma$  can be understood as the superposition of the two trends using a model  $P$  dependence of  $\bar{m}$  and  $\omega_v$ .) Indeed, the present experimental result presented in Figs. 3 and 5 may be explained by this effect.

## V. DISCUSSION

Our calorimetric results in such extreme conditions deserve some discussion, in particular the considerable appar-

ent increase in the specific heat jump at the superconducting transition when  $P_v$  is approached. A very large specific heat jump at  $T_c$  would be strongly reminiscent of the huge value found in  $\text{CeCoIn}_5$ .<sup>48</sup> It is therefore a legitimate question to ask how much the results of the uncalibrated ac calorimetry technique under pressure can be relied on to give an accurate measurement of the specific heat.

The model used to extract the specific heat from the amplitude and phase of the temperature oscillations takes no account of the heat capacity of the solid helium, diamonds, or surrounding pressure apparatus or the essentially three-dimensional nature of the situation. Second, the thermopower of the  $\text{AuFe}$  thermocouple has been assumed not to vary with pressure (Ref. 42 indicates that it varies by no more than 20% up to 12 GPa).

Nevertheless, the superconducting transition observed corresponds to  $\sim 100\%$  of the signal amplitude, indicating that the addenda are a minority contribution to the total signal. Runs at several different frequencies agree to within 10%–20% after the amplitude and phase are combined, with the discrepancy possibly due to frequency-dependent addenda. Kapitza resistance between the sample and helium is likely to better decouple the sample from its surroundings at very low temperature. If the specific heat is calculated using the two-frequency method [Eq. (5)], the result agrees ( $< 5\%$ ) with that calculated using the amplitude and phase up to at least  $2T_c$ . Given these observations, it seems reasonable to accept our results as a good first approximation to  $C_p$ , to within a constant scaling factor, and with an unknown but relatively small component due to addenda.

Furthermore, the apparent anomaly in the normal-state specific heat shown in Fig. 3 was measured at a fixed temperature and frequency above the superconducting transition, with pressure the only independent variable. The small peak in  $\gamma$  is consistent with the maximum in the initial slope of the upper critical field observed at the same pressure, though the interpretation of the latter depends on whether the sample can be considered to be in the clean or dirty limit, or somewhere in between.

Having addressed the experimental questions, let us discuss some other remaining points. The merging of  $T_1^{\text{max}}$  and  $T_2^{\text{max}}$  seems to be a general feature at  $P_v$  in compounds where a critical valence transition is thought to exist. It can be understood as follows.

The so-called Kondo temperature  $T_K$ , related to  $T_i^{\text{max}}$  ( $i = 1, 2$ ), depends crucially on the degeneracy ( $2\ell + 1$ ) of the local  $f$  state:  $T_K \sim D \exp[-1/(2\ell + 1)\rho_F |J|]$ , where  $D$  is the bandwidth of conduction electrons,  $\rho_F$  the density of states of conduction electrons at the Fermi level, and  $J$  the  $c-f$  exchange coupling constant.<sup>49</sup> Even though the sixfold degeneracy of the  $4f$  state is lifted by the CEF effect, leaving the Kramers doublet ground state and excited CEF levels with excitation energy  $\Delta_{\text{CEF}}$ , the Kondo temperature  $T_K$  is still enhanced considerably by the effect of the excited CEF levels.<sup>41</sup>

The technical degeneracy relevant to the Kondo effect is affected by the broadening  $\Delta E$  of the lowest CEF level. If  $\Delta E \ll \Delta_{\text{CEF}}$ , the degeneracy relevant to  $T_K$  is twofold. On the

other hand, if  $\Delta E > \Delta_{\text{CEF}}$ , it increases to fourfold or sixfold. The level broadening is given by  $\Delta E \approx z \pi \rho_F |V|^2$  where  $|V|$  is the strength of  $c-f$  hybridization, and  $z$  is the renormalization factor which gives the inverse of mass enhancement in the case of a lattice system. It is crucial that  $\Delta E$  is very sensitive to the valence of Ce ion because  $z$  is essentially given by  $q$  [Eq. (1)]. In particular, the factor  $z$  increases from a tiny value in the Kondo regime,  $z \sim (1 - n_f) \ll 1$ , and approaches unity in the so-called valence-fluctuation regime.

Since the factor  $\pi \rho_F |V|^2 \gg \Delta_{\text{CEF}}$  in general for Ce-based heavy electron systems, the ratio  $\Delta E / \Delta_{\text{CEF}}$ , which is much smaller than 1 in the Kondo regime, greatly exceeds 1 across the valence transformation around  $P \sim P_v$ , leading to an increase of the technical degeneracy of the  $f$  state, *irrespective* of the sharpness of the valence transformation. Therefore,  $T_1^{\text{max}}$  should merge with  $T_2^{\text{max}}$ , which corresponds to fourfold or sixfold degeneracy of  $4f$  state due to the effect of finite temperature—i.e.,  $T \sim \Delta_{\text{CEF}}$ . This may be the reason why  $T_1^{\text{max}}$  increases and approaches  $T_2^{\text{max}}$  at pressure where  $T_c$  exhibits the maximum, and the KW ratio changes between strongly and weakly correlated classes.

While the experimental picture of  $\text{CeCu}_2\text{Si}_2$  presented in this paper is more complete than the theoretical, a large number of the features found around  $P_v$  follow directly from the valence fluctuation approach and the addition of a  $U_{cf}$  term to the Hamiltonian. The linear resistivity is explained in Sec. IV, as is the local maximum in the electronic specific heat, possibly due to the renormalization of the effective mass due to valence fluctuations, superimposed on an overall decrease with pressure. The enhancement of the residual resistivity at low temperature follows from the renormalization of impurity potentials by valence fluctuations. The relative positions of the peaks in  $T_c$ ,  $\gamma$ , and  $\rho_0$  are consistent with the valence-fluctuation scenario, but for a more precise comparison more detailed calculation would be needed.

Other features yet to be fully addressed with the current model are observed to occur in the valence-fluctuation region. They are the apparent increase in the specific heat jump at  $T_c$ , the temperature dependence of the impurity contribution to the resistivity, and the nature of the superconducting state between the onset and completion of the superconducting transition.

The presence, and indeed enhancement, of superconductivity so far from the disappearance of magnetic order calls into question whether magnetic mediation is really the sole mechanism of superconductivity in  $\text{CeCu}_2\text{Si}_2$ . The evidence presented here, along with other anomalous behavior seen at a pressure well separated from the disappearance of magnetism, strongly suggests the presence of a second quantum critical point in  $\text{CeCu}_2\text{Si}_2$ , this time related to quantum fluctuations between electronic configurations rather than to collective spin instabilities. While magnetic pairing may be responsible for superconductivity at the magnetic QCP, critical valence fluctuations are responsible for pairing at  $P_v$ . The recent result in  $\text{CeCu}_2(\text{Si}_{0.9}\text{Ge}_{0.1})_2$ ,<sup>11</sup> where two separate peaks of  $T_c$  are observed, suggests the validity of the present point of view.

Figure 7 shows a schematic phase diagram for the

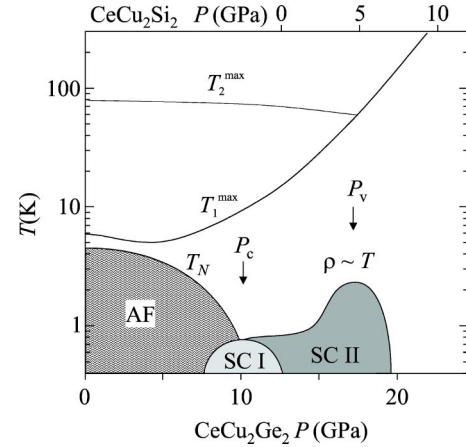


FIG. 7. Schematic  $P-T$  phase diagram for  $\text{CeCu}_2(\text{Si/Ge})_2$  showing the two critical pressures  $P_c$  and  $P_v$ . At  $P_c$ , where the antiferromagnetic ordering temperature  $T_N \rightarrow 0$ , superconductivity in region SC I is mediated by antiferromagnetic spin fluctuations; around  $P_v$ , in region SC II, valence fluctuations provide the pairing mechanism and the resistivity is linear in temperature. The temperatures  $T_1^{\text{max}}$  and  $T_2^{\text{max}}$  merge at a pressure coinciding with  $P_v$ .

$\text{CeCu}_2(\text{Si/Ge})_2$  system. The two critical pressures  $P_c$  and  $P_v$  are, respectively, defined by the disappearance of magnetic order as  $T_N$  tends to zero and by the region of linear resistivity where  $\rho_0$  has a maximum and  $T_1^{\text{max}} \approx T_2^{\text{max}}$ , accompanied by a maximum in  $T_c$ . In  $\text{CeCu}_2\text{Si}_2$  and  $\text{CeCu}_2\text{Ge}_2$  the two critical pressures are widely separated. In compounds such as  $\text{CePd}_2\text{Si}_2$ , on the other hand, superconductivity is found in a narrow pocket, seemingly directly connected to the disappearance of magnetism as  $T_N \rightarrow 0$ . However, many of the other anomalies listed in Table I are still observed in this system and are difficult to explain within a purely spin fluctuation picture. If a valence instability is present in  $\text{CePd}_2\text{Si}_2$ ,  $P_v$  is superimposed on  $P_c$ , as identified by the pressure at which  $T_1^{\text{max}} \approx T_2^{\text{max}}$ .<sup>29</sup> The physics associated with the valence change in  $\text{CeCu}_2\text{Si}_2$  may thus also play an important role in other heavy fermion superconductors. Linear resistivity and an enhancement of  $\rho_0$  have also been seen in the  $\text{CeTIn}_5$  compounds,<sup>48,50</sup> where  $T$  is Co, Rh, or Ir. For this family, superconductivity extends over a relatively broad pressure range, and it may be that valence fluctuations also play a role with a critical valence pressure separate from any magnetic instability.

Valence transitions, such as the Ce  $\alpha-\gamma$  transition, are typically of first order, characterized by an abrupt change in unit cell volume, while retaining its structure. In the case of  $\text{CeCu}_2\text{Si}_2$ , we are proposing that the transition has more of a second-order character. This can be understood from the general point of view as the critical end point of a first-order transition. If this lies at sufficiently low temperature, the ensuing critical excitations can mediate superconductivity without being overwhelmed by thermal fluctuations. More specifically to our theoretical model, in Refs. 22 and 43, it is shown that as the Coulomb repulsion parameter  $U_{cf}$  is increased, the valence transition becomes increasingly steep, eventually approaching a first-order transition.

Finally, it is worth addressing the physical interpretation

of the valence-fluctuation mediated pairing interaction. We emphasize that this intuitive explanation is rather speculative, but we think that it is sufficiently useful to merit inclusion.

A clue comes from the likely nearest-neighbor pairing, implied by the largely local nature of the interaction, and the prediction of  $d$ -wave pairing symmetry. One can imagine an almost filled  $f$  band, with each occupied  $f^1$  site experiencing a Coulomb repulsion  $U_{cf}$  from the respective conduction electrons. As the pressure is increased and  $\epsilon_f$  moves closer to the Fermi level  $\epsilon_F$ , there will come a point where  $\epsilon_f + U_{cf} = \epsilon_F$  and the  $f$  band will start to empty. On an individual  $4f^0$  “hole” site, the  $U_{cf}$  interaction will be absent; thus an increased density of conduction electrons would be energetically favorable at this position. If this extra “screening” conduction electron density is not strictly localized onto the atom itself, but spills onto neighboring sites, the  $f$  electrons on Ce atoms around the original “hole” site will feel an increased repulsion. The tendency to transfer electrons from the  $f$  to conduction bands will be locally reinforced, explaining intuitively the increasingly catastrophic drop in  $n_f$  for larger  $U_{cf}$ , predicted in Ref. 22. For large enough  $U_{cf}$ , phase separation would be expected to occur for some values of  $\epsilon_f$ .

The attractive pairing interaction can be understood as follows: Consider an isolated pair of  $4f^0$  “holes,” accompanied by their cloud of conduction electrons. If these are separated by two lattice positions, with an intervening filled  $4f^1$  site, the two clouds of conduction electrons will overlap at the intermediate site, further increasing the Coulomb energy at that point. It would therefore be energetically favorable for the two “holes” to be on neighboring atoms, thus the attractive interaction. The attractive interaction between “holes” is

equivalent to that between “electrons,” so that this argument would give an intuitive understanding of the origin of the valence-fluctuation mechanism of superconductivity.

## VI. CONCLUSIONS

The enhancement of superconductivity in CeCu<sub>2</sub>Si<sub>2</sub> under pressure is found to coincide with a number of anomalies in the superconducting- and normal-state properties that are hard to explain in a purely spin-fluctuation scenario. Many of these anomalies are directly related to an abrupt change in valence of the Ce ion, while others can be indirectly connected to such a transition. We propose a second critical pressure  $P_v$  at around 4.5 GPa where critical valence fluctuations provide the superconducting pairing mechanism. An extended Anderson lattice model with Coulomb repulsion between the conduction and  $f$  electrons predicts an abrupt change in Ce  $f$  level occupation. The associated fluctuations are sufficient to explain the observed enhancement of  $T_c$ , the  $T$ -linear normal-state resistivity, the enhancement of the residual resistivity, and the peak in the electronic specific heat coefficient  $\gamma$ .

## ACKNOWLEDGMENTS

A.H. and D.J. would like to thank A. Demuer, F. Bouquet, and A. Junod for careful reading of the manuscript and invaluable comments and R. Cartoni for technical assistance. One of the authors (K.M.) acknowledges stimulating communications with H.Q. Yuan and F. Steglich. K.M. was supported in part by a Grant-in-Aid for Creative Scientific Research and the 21st Century COE Program by the Japan Society for the Promotion of Science.

\*alexander.holmes@physics.unige.ch

†didier.jaccard@physics.unige.ch

‡miyake@mp.es.osaka-u.ac.jp

<sup>1</sup>F. Steglich, J. Aarts, C. D. Bredl, W. Lieke, D. Meschede, W. Franz, and H. Schafer, Phys. Rev. Lett. **43**, 1892 (1979).

<sup>2</sup>N. D. Mathur, F. M. Grosche, S. R. Julian, I. R. Walker, D. M. Freye, R. K. W. Haselwimmer, and G. G. Lonzarich, Nature (London) **394**, 39 (1998).

<sup>3</sup>K. Miyake, S. Schmitt-Rink, and C. M. Varma, Phys. Rev. B **34**, 6554 (1986).

<sup>4</sup>D. J. Scalapino, E. Loh, and J. E. Hirsch, Phys. Rev. B **34**, 8190 (1986).

<sup>5</sup>P. Monthoux and G. G. Lonzarich, Phys. Rev. B **66**, 224504 (2002).

<sup>6</sup>Y. Kawasaki, K. Ishida, T. Mito, C. Thessieu, G.-q. Zheng, Y. Kitaoka, C. Geibel, and F. Steglich, Phys. Rev. B **63**, 140501 (2001).

<sup>7</sup>S. Kawasaki *et al.*, Phys. Rev. B **65**, 020504 (2002).

<sup>8</sup>Y. Fuseya, H. Kohno, and K. Miyake, J. Phys. Soc. Jpn. **72**, 2914 (2003).

<sup>9</sup>K. Miyake, O. Narikiyo, and Y. Onishi, Physica B **259–261**, 676 (1999).

<sup>10</sup>D. Jaccard, H. Wilhelm, K. Alami-Yadri, and E. Vargoz, Physica B **259–261**, 1 (1999).

<sup>11</sup>H. Q. Yuan, M. Deppe, G. Sparn, C. Geibel, and F. Steglich, Acta Phys. Pol. B **34**, 533 (2003).

<sup>12</sup>B. Bellarbi, A. Benoit, D. Jaccard, J. M. Mignot, and H. F. Braun, Phys. Rev. B **30**, 1182 (1984).

<sup>13</sup>F. Thomas, C. Ayache, I. A. Fomine, J. Thomasson, and C. Geibel, J. Phys.: Condens. Matter **8**, L51 (1996).

<sup>14</sup>E. Vargoz, D. Jaccard, J. Y. Genoud, J. P. Brison, and J. Flouquet, Solid State Commun. **106**, 631 (1998).

<sup>15</sup>J. Thomasson, Y. Okayama, I. Sheikin, J. P. Brison, and D. Braithwaite, Solid State Commun. **106**, 637 (1998).

<sup>16</sup>E. Vargoz and D. Jaccard, J. Magn. Magn. Mater. **177–181**, 294 (1998).

<sup>17</sup>T. M. Rice and K. Ueda, Phys. Rev. B **34**, 6420 (1986).

<sup>18</sup>H. Shiba, Phys. Soc. Jpn. **55**, 2765 (1986).

<sup>19</sup>K. Kadowaki and S. Woods, Solid State Commun. **58**, 507 (1986).

<sup>20</sup>K. Miyake, T. Matsuura, and C. M. Varma, Solid State Commun. **71**, 1149 (1989).

<sup>21</sup>K. Miyake and H. Maebashi, J. Phys. Soc. Jpn. **71**, 1007 (2002).

<sup>22</sup>Y. Onishi and K. Miyake, J. Phys. Soc. Jpn. **69**, 3955 (2000).

<sup>23</sup>A. Onodera, S. Tsuduki, Y. Ohishi, T. Watanuki, K. Ishida, Y. Kitaoka, and Y. Onuki, Solid State Commun. **123**, 113 (2002).

<sup>24</sup>J. Roehler, J. Klug, and K. Keulertz, J. Magn. Magn. Mater. **76–77**, 340 (1988).

- <sup>25</sup>D. Jaccard, J. M. Mignot, B. Bellarbi, A. Benoit, H. F. Braun, and J. Sierro, *J. Magn. Magn. Mater.* **47–48**, 23 (1985).
- <sup>26</sup>D. Jaccard, E. Vargoz, K. Alami-Yadri, and H. Wilhelm, *Rev. High Press Sci. Technol.* **7**, 412 (1998).
- <sup>27</sup>E. Vargoz, Ph.D. thesis, University of Geneva, 1998.
- <sup>28</sup>P. Link, D. Jaccard, and P. Lejay, *Physica B* **225**, 207 (1996).
- <sup>29</sup>A. Demuer, A. T. Holmes, and D. Jaccard, *J. Phys.: Condens. Matter* **14**, L529 (2002).
- <sup>30</sup>H. Wilhelm, S. Raymond, D. Jaccard, O. Stockert, H. v. Loehneysen, and A. Rosch, in *Proceedings of AIRAPT-17, Hawaii, 1999*, edited by M. Manghnani, W. Nellis, and M. Nicol (Universities Press, Hyderabad, 2000), pp. 697–700.
- <sup>31</sup>M. Ishikawa, H. F. Braun, and J. L. Jorda, *Phys. Rev. B* **27**, 3092 (1983).
- <sup>32</sup>F. Steglich *et al.*, *Physica B* **223–224**, 1 (1996).
- <sup>33</sup>D. Louca, J. D. Thompson, J. M. Lawrence, R. Movshovich, C. Petrovic, J. L. Sarrao, and G. H. Kwei, *Phys. Rev. B* **61**, R14 940 (2000).
- <sup>34</sup>M. I. Eremets, *High Pressure Experimental Methods* (Oxford University Press, Oxford, 1996).
- <sup>35</sup>A. Eichler and W. Gey, *Rev. Sci. Instrum.* **50**, 1445 (1979).
- <sup>36</sup>A. T. Holmes, A. Demuer, and D. Jaccard, *Acta Phys. Pol. B* **34**, 567 (2003).
- <sup>37</sup>See, for example, T. Tsuneto, *Superconductivity and Superfluidity* (Cambridge University Press, Cambridge, England, 1998), Sec. 4.5.4.
- <sup>38</sup>D. Braithwaite (private communication).
- <sup>39</sup>D. Cox and N. Grewe, *Z. Phys. B*: **71**, 321 (1988).
- <sup>40</sup>B. Cornut and B. Coqblin, *Phys. Rev. B* **5**, 4541 (1972).
- <sup>41</sup>K. Yamada, K. Yosida, and K. Hanzawa, *Prog. Theor. Phys.* **71**, 450 (1984).
- <sup>42</sup>H. Wilhelm and D. Jaccard, *Phys. Rev. B* **66**, 064428 (2002).
- <sup>43</sup>Y. Onishi and K. Miyake, *Physica B* **281–282**, 191 (2000).
- <sup>44</sup>C. M. Varma, P. B. Littlewood, S. Schmitt-Rink, E. Abrahams, and A. E. Ruckenstein, *Phys. Rev. Lett.* **63**, 1996 (1989).
- <sup>45</sup>C. M. Varma, S. Schmitt-Rink, and E. Abrahams, *Solid State Commun.* **62**, 681 (1987).
- <sup>46</sup>I. E. Perakis, C. M. Varma, and A. E. Ruckenstein, *Phys. Rev. Lett.* **70**, 3467 (1993).
- <sup>47</sup>C. M. Varma, Z. Nussinov, and W. van Saarloos, *Phys. Rep.* **361**, 267 (2002).
- <sup>48</sup>C. Petrovic, P. G. Pagliuso, M. F. Hundley, R. Movshovich, J. L. Sarrao, J. D. Thompson, Z. Fisk, and P. Monthoux, *J. Phys.: Condens. Matter* **13**, L337 (2001).
- <sup>49</sup>I. Okada and K. Yosida, *Prog. Theor. Phys.* **49**, 1483 (1973).
- <sup>50</sup>T. Muramatsu, N. Tateiwa, T. C. Kobayashi, K. Shimizu, K. Amaya, D. Aoki, H. Shishido, Y. Haga, and Y. Onuki, *J. Phys. Soc. Jpn.* **70**, 3362 (2001).